

Efficient Bayesian hierarchical functional data analysis with basis function approximations using Gaussian-Wishart processes

Jingjing Yang

Department of Biostatistics, University of Michigan, Ann Arbor, MI 48109, USA.

email: yjingj@umich.edu

and

Dennis D. Cox

Department of Statistics, Rice University, Houston, TX 77005, USA.

and

Jong Soo Lee

Department of Mathematical Sciences, University of Massachusetts Lowell, Lowell, MA 01854, USA.

and

Peng Ren

Suntrust Banks Inc, Atlanta, GA 30308, USA.

and

Taeryon Choi

Department of Statistics, Korea University, Seoul 136-701, Republic of Korea.

email: trchoi@korea.ac.kr

SUMMARY: Functional data are defined as realizations of random functions (mostly smooth functions) varying over a continuum, which are usually collected with measurement errors on discretized grids. In order to accurately smooth noisy functional observations and deal with the issue of high-dimensional observation grids, we propose a novel Bayesian method based on the Bayesian hierarchical model with a Gaussian-Wishart process prior and basis function representations. We first derive an induced model for the basis-function coefficients of the functional data, and then use this model to conduct posterior inference through Markov chain Monte Carlo. Compared to the standard Bayesian inference that suffers serious computational burden and unstableness for analyzing high-dimensional functional data, our method greatly improves the computational scalability

000 0000

and stability, while inheriting the advantage of simultaneously smoothing raw observations and estimating the mean-covariance functions in a nonparametric way. In addition, our method can naturally handle functional data observed on random or uncommon grids. Simulation and real studies demonstrate that our method produces similar results as the standard Bayesian inference with low-dimensional common grids, while efficiently smoothing and estimating functional data with random and high-dimensional observation grids where the standard Bayesian inference fails. In conclusion, our method can efficiently smooth and estimate high-dimensional functional data, providing one way to resolve the curse of dimensionality for Bayesian functional data analysis with Gaussian-Wishart processes.

KEY WORDS: basis function; Bayesian hierarchical model; functional data analysis; Gaussian-Wishart process; smoothing;

1. Introduction

Functional data — defined as realizations of random functions varying over a continuum (Ramsay and Silverman, 2005) — include a variety of data types such as longitudinal data, spatial-temporal data, and image data. Because functional data are generally collected on discretized grids with measurement errors, constructing functions from noisy discrete observations (referred to as smoothing) is an essential step for analyzing functional data (Ramsay and Dalzell, 1991; Ramsay and Silverman, 2005). However, the smoothing step has been neglected by most of the existing functional data analysis (FDA) methods, which integrate functional representations in the analysis models. For examples, functional data and effects are represented by basis functions in functional linear regression models (Cardot et al., 1999, 2003; Hall et al., 2007; Zhu and Cox, 2009; Zhu et al., 2011), functional additive models (Scheipl et al., 2015; Fan et al., 2015), functional principle components analysis (Crainiceanu and Goldsmith, 2010; Zhu et al., 2014), and nonparametric functional regression models (Ferraty and Vieu, 2006; Gromenko and Kokoszka, 2013); and represented by Gaussian processes (GP) in Bayesian nonparametric models (Gibbs, 1998; Shi et al., 2007; Banerjee et al., 2008; Kaufman and Sain, 2010).

On the other hand, most of the existing smoothing methods process one functional observation per time, such as cubic smoothing splines (CSS) and kernel smoothing (Green and Silverman, 1993; Ramsay and Silverman, 2005). Consequently, when multiple functional observations are sampled from the same distribution, these individually smoothing methods lead to less accurate results, by ignoring the shared mean-covariance functions. Alternatively, Yang et al. (2016) proposed a Bayesian hierarchical model (BHM) with Gaussian-Wishart processes for simultaneously and nonparametrically smoothing multiple functional observations and estimating mean-covariance functions, which is shown to be comparable with the frequentist method — Principle Analysis by Conditional Expectation (PACE) proposed by Yao et al. (2005b).

BHM assumes a general measurement error model for the observed functional data $\{Y_i(t); t \in$

$\mathcal{T}, i = 1, \dots, n\}$,

$$\begin{aligned} Y_i(t) &= Z_i(t) + \epsilon_i(t); \quad Z_i(\cdot) \sim GP(\mu_Z(\cdot), \Sigma_Z(\cdot, \cdot)), \quad \epsilon_i(\cdot) \sim N(0, \sigma_\epsilon^2); \\ \mu_Z(\cdot) | \Sigma_Z(\cdot, \cdot) &\sim GP\left(\mu_0(\cdot), \frac{1}{c}\Sigma_Z(\cdot, \cdot)\right), \quad \Sigma_Z(\cdot, \cdot) \sim IWP(\delta, \sigma_s^2 A(\cdot, \cdot)), \quad \sigma_\epsilon^2 \sim IG(a_\epsilon, b_\epsilon); \\ \sigma_s^2 &\sim IG(a_s, b_s); \end{aligned} \quad (1)$$

where $\{Z_i(t); i = 1, \dots, n\}$ denotes the underlying true functional data following the same GP distribution with mean function $\mu_Z(\cdot)$ and covariance function $\Sigma_Z(\cdot, \cdot)$, *IWP* denotes the Inverse-Wishart process (IWP) prior (Dawid, 1981) for the covariance function, *IG* denotes the Inverse-Gamma prior, and $(\mu_0(\cdot), c, \delta, A(\cdot, \cdot), a_\epsilon, b_\epsilon, a_s, b_s)$ are hyper-prior parameters to be determined. The IWP prior on $\Sigma_Z(\cdot, \cdot)$ models the covariance function nonparametrically and hence allows the method for analyzing both stationary and nonstationary functional data with unknown covariance structures.

However, the BHM suffers serious computational burden and instability when functional data are observed on high-dimensional or random grids. To address the computational issue of Bayesian GP regression models for high-dimensional functional data, the existing reduce-rank methods focus on kriging with partial data (Cressie and Johannesson, 2008; Banerjee et al., 2008), implementing direct low-rank approximations for the covariance matrix (Rasmussen and Williams, 2006; Quiñonero Candela et al., 2007; Shi and Choi, 2011; Banerjee et al., 2013), and using predictive processes (Sang and Huang, 2012; Finley et al., 2015). Although these reduce-rank methods successfully apply to the standard GP regression models (Shi et al., 2007; Banerjee et al., 2008; Kaufman and Sain, 2010) that only model group-level GPs with parametric covariance functions, they greatly increase the complexity in BHM for handling multiple GPs (one per functional observation, one for the mean prior) and an IWP (prior for the covariance function).

In this paper, we propose a novel **B**ayesian framework with **A**pproximations by **B**asis **F**unctions for the original BHM method, referred to as **BABF**, which is computationally efficient and stable for analyzing high-dimensional functional data. Basically, we approximate the underlying true

functional data $\{Z_i(t); i = 1, \dots, n\}$ with basis functions, and derive an induced Bayesian hierarchical model on the basis-function coefficients from the original assumptions of BHM (1). Then we can conduct posterior inference for functional signals $\{Z_i(t); i = 1, \dots, n\}$ and mean-covariance functions $(\mu_Z(\cdot), \Sigma_Z(\cdot, \cdot))$, by Markov chain Monte Carlo (MCMC) under the induced model of basis-function coefficients, i.e., by MCMC in the basis-function space with a reduced rank. As a result, our BABF method not only improves the computational scalability over the original BHM, but also inherits the advantage of modeling the functional data and mean-covariance functions in a flexible nonparametric manner. In addition, because of basis function approximations, BABF can naturally handle functional data observed on random or uncommon grids.

Thus, our basis function approximation approach has two-fold advantages: (i) Compared to the alternative reduce-rank approaches, it is easier to apply to Bayesian hierarchical GP methods that model individual levels of GPs (e.g., BHM). (ii) It induces a nonparametric Bayesian model with a Gaussian-Wishart prior for the basis-function coefficients, which is different from modeling the basis-function coefficients as independent variables as in the standard functional linear regression models (Cardot et al., 1999, 2003; Hall et al., 2007; Zhu and Cox, 2009; Zhu et al., 2011) and functional additive models (Scheipl et al., 2015; Fan et al., 2015), and also different from directly modeling the basis-function coefficients in semiparametric forms as in Baladandayuthapani et al. (2008).

By simulation studies with both stationary and nonstationary functional data, we demonstrate that BABF produces accurate smoothing results and mean-covariance function estimates. Specifically, when functional data are observed on low-dimensional common grids, BABF generates similar results as the original BHM. When functional data are observed on high-dimensional or random grids, the original BHM fails because of computational issues,

while BABF efficiently produces smoothed signal estimates with smaller root mean square errors (RMSEs) than the alternative methods (CSS, PACE).

Furthermore, by a real study with the sleeping energy expenditure (SEE) measurements of 106 children and adolescents (44 obese cases, 62 controls) over 405 time points (Lee et al., 2016), we show that BABF captures better periodic patterns of the measurements, producing more reasonable estimates for the functional signals and mean-covariance functions. Moreover, compared to the raw data and smoothed data by CSS and PACE, the smoothed data by BABF leads to better classification results for the SEE data.

This paper is organized as follows: We describe the BABF method in Section 2, present simulation and real studies in Sections 3 and 4 respectively, and then conclude with a discussion in Section 5.

2. BABF method

Because the original BHM method (Yang et al., 2016) conducts MCMC on the pooled observation grid for handling uncommon grids, it has computational complexity $O(np^3m)$ with n samples, p pooled-grid points, and m MCMC iterations. To resolve the computational bottleneck issue for smoothing functional data with large pooled-grid dimension p by BHM, we propose our BABF method by approximating functional data with basis functions under the same model assumptions as in BHM (1).

2.1 Model description

First, we approximate the GP evaluations $\{Z_i(\tau)\}$ by a system of basis functions (e.g., cubic B-splines), with a working grid based on data density, $\tau = (\tau_1, \tau_2, \dots, \tau_L)^T \subset \mathcal{T}$, $L \ll p$. Let $B(\cdot) = [b_1(\cdot), b_2(\cdot), \dots, b_K(\cdot)]$ denote K selected basis functions with coefficients $\zeta_i = (\zeta_{i1}, \zeta_{i2}, \dots, \zeta_{iK})^T$, then

$$Z_i(\tau) = \sum_{k=1}^K \zeta_{ik} b_k(\tau) = B(\tau) \zeta_i. \quad (2)$$

Assuming $K = L$, we can write $\zeta_i = \mathbf{B}(\boldsymbol{\tau})^{-1} Z_i(\boldsymbol{\tau})$ as a linear transformation of $Z_i(\boldsymbol{\tau})$. Note that even if $\mathbf{B}(\boldsymbol{\tau})$ is singular or non-square, ζ_i can still be written as a linear transformation of $Z_i(\boldsymbol{\tau})$ with the generalized inverse (James, 1978) of $\mathbf{B}(\boldsymbol{\tau})$. Consequently, the true signals $\{Z_i(\mathbf{t}_i)\}$ can be approximated by $\{\mathbf{B}(\mathbf{t}_i)\zeta_i\}$ with given $\{\zeta_i\}$.

Second, we derive the induced Bayesian hierarchical model for the basis-function coefficients $\{\zeta_i\}$. Because ζ_i is a linear transformation of $Z_i(\boldsymbol{\tau})$ that follows a multivariate normal distribution $MN(\mu_Z(\boldsymbol{\tau}), \Sigma_Z(\boldsymbol{\tau}, \boldsymbol{\tau}))$ under the assumptions in (1), the induced model for ζ_i is

$$\zeta_i \sim MN(\boldsymbol{\mu}_\zeta, \boldsymbol{\Sigma}_\zeta); \boldsymbol{\mu}_\zeta = \mathbf{B}(\boldsymbol{\tau})^{-1} \mu_Z(\boldsymbol{\tau}); \boldsymbol{\Sigma}_\zeta = \mathbf{B}(\boldsymbol{\tau})^{-1} \Sigma_Z(\boldsymbol{\tau}, \boldsymbol{\tau}) \mathbf{B}(\boldsymbol{\tau})^{-T}. \quad (3)$$

Further, from the assumed priors of $(\mu_Z(\cdot), \Sigma_Z(\cdot, \cdot))$ in (1), the following priors of $(\boldsymbol{\mu}_\zeta, \boldsymbol{\Sigma}_\zeta)$ are also induced:

$$\boldsymbol{\mu}_\zeta | \boldsymbol{\Sigma}_\zeta \sim MN(\mathbf{B}(\boldsymbol{\tau})^{-1} \mu_0(\boldsymbol{\tau}), c \boldsymbol{\Sigma}_\zeta); \quad (4)$$

$$\boldsymbol{\Sigma}_\zeta \sim IW(\delta, \mathbf{B}(\boldsymbol{\tau})^{-1} \Psi(\boldsymbol{\tau}, \boldsymbol{\tau}) \mathbf{B}(\boldsymbol{\tau})^{-T}). \quad (5)$$

Last, we conduct MCMC by a Gibbs-Sampler (Geman and Geman, 1984) with computation complexity $O(nK^3m)$ under the above induced model of the basis-function coefficients. Details of the MCMC procedure are provided in Section 2.4.3. We take the corresponding averages of the posterior MCMC samples as our Bayesian estimates, whose uncertainties can easily be quantified by the MCMC credible intervals.

2.2 Hyper-prior selection

For setting hyper-priors, we use the same data-driven strategy as used by the original BHM method (Yang et al., 2016). Specifically, we set $\mu_0(\cdot)$ as the smoothed sample mean, and $c = 1$, $\delta = 5$ for uninformative priors of the mean-covariance functions. We set $A(\cdot, \cdot)$ as a Matérn covariance function (Matérn, 1960) for stationary data, or as a smooth covariance estimate for nonstationary data (e.g., PACE estimate, smoothed empirical estimate). A heuristic Bayesian approach is used for setting the values of $(a_\epsilon, b_\epsilon, a_s, b_s)$, by matching hyper-prior moments with the empirical estimates.

2.3 Basis-function selection

The key feature of the BABF method is conducting MCMC with the induced model of the basis-function coefficients. BABF inherits the advantage of nonparametrically smoothing without the necessity of tuning smoothing parameters, where the amount of smoothness in the posterior estimates is determined by the data and the IWP prior of the covariance function. Therefore, the induced model of the basis-function coefficients makes BABF robust with respect to the selected basis functions and working grid.

Moreover, the appropriately selected basis functions and working grid will help improve the performance of BABF. The general strategies of selecting basis functions for interpolating over the working grid apply here, where the basis-function type depends on the data, e.g., Fourier series for periodic data, B-splines for GP data, and wavelets for signal data. Using B-splines as an example, the optimal knot sequence for best interpolation at the working grid τ can be obtained using the method developed by Gaffney and Powell (1976); Micchelli et al. (1976); de Boor (1977), and implemented by the Matlab function `optknt`. The working grid τ can be chosen to represent data densities over the domain, e.g., given by the $(\frac{1}{L+1}, \dots, \frac{L}{L+1})$ percentiles of the pooled observation grid, or the equally-spaced grid for evenly distributed data. As for the dimension L of the working grid, one may try a few values with a small testing data set, and then select one with the smallest RMSE of the signal estimates.

2.4 Posterior inference

For the original BHM (1), the joint posterior distribution of $(\mathbf{Z}, \mu_Z, \Sigma_Z, \sigma_\epsilon^2, \sigma_s^2)$ is

$$f(\mathbf{Z}, \mu_Z, \Sigma_Z, \sigma_\epsilon^2, \sigma_s^2 | \mathbf{Y}) \propto f(\mathbf{Y} | \mathbf{Z}, \sigma_\epsilon^2) f(\mathbf{Z} | \mu_Z, \Sigma_Z) f(\mu_Z | \Sigma_Z) f(\Sigma_Z | \sigma_\epsilon^2) f(\sigma_\epsilon^2) f(\sigma_s^2), \quad (6)$$

$$\mathbf{Z} = \{Z_1(\mathbf{t}_i), \dots, Z_n(\mathbf{t}_n)\}, \quad \mathbf{Y} = \{Y_1(\mathbf{t}_i), \dots, Y_n(\mathbf{t}_n)\}.$$

Equivalently, because of $\zeta_i = \mathbf{B}(\boldsymbol{\tau})^{-1} Z_i(\boldsymbol{\tau})$, the joint posterior distribution of $(\boldsymbol{\zeta}, \boldsymbol{\mu}_\zeta, \boldsymbol{\Sigma}_\zeta, \sigma_\epsilon^2, \sigma_s^2)$ is

$$f(\boldsymbol{\zeta}, \boldsymbol{\mu}_\zeta, \boldsymbol{\Sigma}_\zeta, \sigma_\epsilon^2, \sigma_s^2 | \mathbf{Y}) \propto f(\mathbf{Y} | \boldsymbol{\zeta}, \sigma_\epsilon^2) f(\boldsymbol{\zeta} | \boldsymbol{\mu}_\zeta, \boldsymbol{\Sigma}_\zeta) f(\boldsymbol{\mu}_\zeta | \boldsymbol{\Sigma}_\zeta) f(\boldsymbol{\Sigma}_\zeta | \sigma_s^2) f(\sigma_\epsilon^2) f(\sigma_s^2), \quad (7)$$

$$\boldsymbol{\zeta} = \{\zeta_1, \dots, \zeta_n\}, \quad \boldsymbol{\mu}_\zeta = \mathbf{B}(\boldsymbol{\tau})^{-1} \mu_Z(\boldsymbol{\tau}), \quad \boldsymbol{\Sigma}_\zeta = \mathbf{B}(\boldsymbol{\tau})^{-1} \Sigma_Z(\boldsymbol{\tau}, \boldsymbol{\tau}) \mathbf{B}(\boldsymbol{\tau})^{-T}.$$

2.4.1 *Full conditional distribution of ζ_i .* From (7), we can see that

$$f(\zeta_i | \mathbf{Y}, \boldsymbol{\mu}_\zeta, \boldsymbol{\Sigma}_\zeta) \propto f(\mathbf{Y} | \boldsymbol{\zeta}, \sigma_\epsilon^2) f(\boldsymbol{\zeta} | \boldsymbol{\mu}_\zeta, \boldsymbol{\Sigma}_\zeta).$$

Then the full conditional posterior distribution of ζ_i is derived as

$$\zeta_i | (Y_i(\mathbf{t}_i), \boldsymbol{\mu}_\zeta, \boldsymbol{\Sigma}_\zeta) \sim MN [\mathbf{m}_{\zeta_i | Y_i}, \mathbf{V}_{\zeta_i | Y_i}]; \quad (8)$$

$$\mathbf{V}_{\zeta_i | Y_i} = \left(\frac{\mathbf{B}(\mathbf{t}_i)^T \mathbf{B}(\mathbf{t}_i)}{\sigma_\epsilon^2} + \boldsymbol{\Sigma}_\zeta^{-1} \right)^{-1}, \quad \mathbf{m}_{\zeta_i | Y_i} = \mathbf{V}_{\zeta_i | Y_i} \left(\frac{\mathbf{B}(\mathbf{t}_i)^T Y_i(\mathbf{t}_i)}{\sigma_\epsilon^2} + \boldsymbol{\Sigma}_\zeta^{-1} \boldsymbol{\mu}_\zeta \right).$$

2.4.2 *Full conditional distribution for $\boldsymbol{\mu}_\zeta, \boldsymbol{\Sigma}_\zeta$.* Conditioning on $\{\zeta_i\}$, the posterior distribution of $(\boldsymbol{\mu}_\zeta, \boldsymbol{\Sigma}_\zeta)$ is

$$f(\boldsymbol{\mu}_\zeta, \boldsymbol{\Sigma}_\zeta | \zeta_1, \dots, \zeta_n) \propto \prod_{i=1}^n f(\zeta_i | \boldsymbol{\mu}_\zeta, \boldsymbol{\Sigma}_\zeta) f(\boldsymbol{\mu}_\zeta | \boldsymbol{\Sigma}_\zeta) f(\boldsymbol{\Sigma}_\zeta),$$

where $f(\boldsymbol{\mu}_\zeta | \boldsymbol{\Sigma}_\zeta)$ and $f(\boldsymbol{\Sigma}_\zeta)$ are given by (4), (5). Therefore,

$$\boldsymbol{\mu}_\zeta | (\zeta_1, \dots, \zeta_n, \boldsymbol{\Sigma}_\zeta) \sim MN \left(\frac{1}{n+c} \left(\sum_{i=1}^n \zeta_i + c \mathbf{B}(\boldsymbol{\tau})^{-1} \mu_0(\boldsymbol{\tau}) \right), \frac{1}{n+c} \boldsymbol{\Sigma}_\zeta \right); \quad (9)$$

$$\boldsymbol{\Sigma}_\zeta | (\zeta_1, \dots, \zeta_n, \boldsymbol{\mu}_\zeta) \sim IW(\tilde{\delta}_\zeta, \tilde{\boldsymbol{\Psi}}_\zeta), \quad (10)$$

$$\tilde{\delta}_\zeta = n + 1 + \delta, \quad \tilde{\boldsymbol{\Psi}}_\zeta = \sum_{i=1}^n (\zeta_i - \boldsymbol{\mu}_\zeta)(\zeta_i - \boldsymbol{\mu}_\zeta)^T +$$

$$c(\boldsymbol{\mu}_\zeta - \mathbf{B}(\boldsymbol{\tau})^{-1} \mu_0(\boldsymbol{\tau}))(\boldsymbol{\mu}_\zeta - \mathbf{B}(\boldsymbol{\tau})^{-1} \mu_0(\boldsymbol{\tau}))^T + \mathbf{B}(\boldsymbol{\tau})^{-1} \boldsymbol{\Psi}(\boldsymbol{\tau}, \boldsymbol{\tau}) \mathbf{B}(\boldsymbol{\tau})^{-T}.$$

2.4.3 *MCMC procedure.* We design the following Gibbs-Sampler algorithm for MCMC, which ensures computational convenience and posterior convergence.

Step 0: Set hyper-priors (Section 2.2) and initial parameter values. Initial values for $(\mu_Z(\boldsymbol{\tau}), \Sigma_Z(\boldsymbol{\tau}, \boldsymbol{\tau}), \sigma_\epsilon^2)$ can be set as empirical estimates, inducing the initial values for $(\boldsymbol{\mu}_\zeta, \boldsymbol{\Sigma}_\zeta)$ by (3).

Step 1: Conditioning on observed data \mathbf{Y} and the current values of $(\boldsymbol{\mu}_\zeta, \boldsymbol{\Sigma}_\zeta, \sigma_\epsilon^2)$, sample $\{\boldsymbol{\zeta}_i\}$ from (8).

Step 2: Conditioning on the current values of $\boldsymbol{\zeta}$, update $\boldsymbol{\mu}_\zeta$ and $\boldsymbol{\Sigma}_\zeta$ respectively from (9) and (10).

Step 3: Given the current values of $(\{\boldsymbol{\zeta}_i\}, \boldsymbol{\mu}_\zeta, \boldsymbol{\Sigma}_\zeta)$, approximate $\{Z_i(\mathbf{t}_i), \mu_Z(\mathbf{t}_i), \Sigma_Z(\mathbf{t}_i, \mathbf{t}_i), \Sigma(\boldsymbol{\tau}, \mathbf{t}_i), \Sigma_Z(\mathbf{t}_i, \boldsymbol{\tau}), \Sigma_Z(\boldsymbol{\tau}, \boldsymbol{\tau})\}$ by

$$\begin{aligned} Z_i(\mathbf{t}_i) &= \mathbf{B}(\mathbf{t}_i)\boldsymbol{\zeta}_i, \quad \mu_Z(\mathbf{t}_i) = \mathbf{B}(\mathbf{t}_i)\boldsymbol{\mu}_\zeta, \quad \Sigma(\mathbf{t}_i, \mathbf{t}_i) = \mathbf{B}(\mathbf{t}_i)\boldsymbol{\Sigma}_\zeta\mathbf{B}(\mathbf{t}_i)^T, \\ \Sigma(\boldsymbol{\tau}, \mathbf{t}_i)^T &= \Sigma(\mathbf{t}_i, \boldsymbol{\tau}) = \mathbf{B}(\mathbf{t}_i)\boldsymbol{\Sigma}_\zeta\mathbf{B}(\boldsymbol{\tau})^T, \quad \Sigma(\boldsymbol{\tau}, \boldsymbol{\tau}) = \mathbf{B}(\boldsymbol{\tau})\boldsymbol{\Sigma}_\zeta\mathbf{B}(\boldsymbol{\tau})^T. \end{aligned}$$

Step 4: Conditioning on \mathbf{Z} and \mathbf{Y} , update σ_ϵ^2 by

$$IG\left(a_\epsilon + \frac{1}{2} \sum_{i=1}^n p_i, \quad b_\epsilon + \frac{1}{2} \sum_{i=1}^n (Y_i(\mathbf{t}_i) - Z_i(\mathbf{t}_i))^T (Y_i(\mathbf{t}_i) - Z_i(\mathbf{t}_i))\right),$$

which is derived from

$$f(\sigma_\epsilon^2 | Y_1(\mathbf{t}_1), Z_1(\mathbf{t}_1), \dots, Y_n(\mathbf{t}_n), Z_n(\mathbf{t}_n)) \propto \prod_{i=1}^n f(Y_i(\mathbf{t}_i) | Z_i(\mathbf{t}_i), \sigma_\epsilon^2) f(\sigma_\epsilon^2).$$

Step 5: Given the current value of $\boldsymbol{\Sigma}_\tau = \Sigma_Z(\boldsymbol{\tau}, \boldsymbol{\tau})$, update σ_s^2 by

$$\sigma_s^2 | \boldsymbol{\Sigma}_\tau \sim G\left(a_s + \frac{(\delta + K - 1)K}{2}, \quad b_s + \frac{1}{2} \text{trace}(\mathbf{A}(\boldsymbol{\tau}, \boldsymbol{\tau})\boldsymbol{\Sigma}_\tau^{-1})\right),$$

which is derived from

$$f(\sigma_s^2 | \boldsymbol{\Sigma}_\tau) \propto f(\boldsymbol{\Sigma}_\tau | \sigma_s^2) f(\sigma_s^2).$$

In general, the posterior samples will pass the convergence diagnosis by potential scale reduction factor (PSRF) (Gelman and Rubin, 1992), with a fairly large number of MCMC iterations (e.g., 12,000 in our numerical studies).

3. Simulation studies

In the following simulation studies, we compared the BABF method with CSS (Green and Silverman, 1993), PACE (Yao et al., 2005a), Bayesian functional principle component analysis (BFPCA) (Crainiceanu and Goldsmith, 2010), standard Bayesian GP regression (BGP) (Gibbs, 1998), and the original BHM method (Yang et al., 2016). We considered scenarios with

stationary and nonstationary functional data, common and random observation grids, Gaussian and non-Gaussian data. Because both BFPCA and BGP are developed for the scenario with common grids; BHM has computational issues with high-dimensional pooled-grid (the case with random grids); and BHM is known to be comparable with PACE (Yang et al., 2016). We compared all methods in the scenario with common grids, but only compared BABF with CSS and PACE in the scenario with random grids.

Because simulation data were evenly distributed over the domain, we selected an equally spaced working grid with length 20 for BABF. CSS was applied to each functional observation independently with the smoothing parameter selected by general cross-validation (GCV). For BFPCA, we used the covariance estimate by PACE, and selected the number of principle functions subject to capture 99.99% data variance. For BGP, we assumed the Matérn model for the covariance function with stationary data, while fixing the covariance at the PACE estimate with nonstationary data. All MCMC samples consisted of 2,000 burn-ins and 10,000 posterior samples, and passed the convergence diagnoses by PSRF (Gelman and Rubin, 1992).

3.1 Studies with common grids

We generated 30 stationary functional curves (true signals) on the common equally-spaced-grid with length 40, over $\mathcal{T} = (0, \pi/2)$, from

$$GP(\mu(t) = 3 \sin(4t), \Sigma(s, t) = 5 \text{Matern}_{cor}(|s - t|; \rho = 0.5, \nu = 3.5)), \quad (11)$$

denoted by \mathbf{Z} . Specifically,

$$\text{Matern}_{cor}(d; \rho, \nu) = \frac{1}{\Gamma(\nu)2^{\nu-1}} \left(\sqrt{2\nu} \frac{d}{\rho} \right)^\nu K_\nu \left(\sqrt{2\nu} \frac{d}{\rho} \right), d \geq 0, \rho > 0, \nu > 0,$$

where ρ is the scale parameter, ν is the order of smoothness, $\Gamma(\cdot)$ is the gamma function, and $K_\nu(\cdot)$ is the modified Bessel function of the second kind. The noise terms $\{\epsilon_{ij}\}$ were generated from $N(0, \sigma_\epsilon = \sqrt{5}/2)$, such that the signal to noise ratio (SNR) was 2 (resulting relatively high volume of noise in the simulated data). The observed noisy functional data curves were given by $\mathbf{Y} = \mathbf{Z} + \boldsymbol{\epsilon}$.

Similarly, we generated 30 nonstationary functional curves on the same equally-spaced-grid with length 40, from a nonstationary GP $\tilde{X}(t) = h(t)X(s(t))$ (i.e., a nonlinear transformation of a stationary GP $X(\cdot)$), where $X(\cdot)$ denotes the GP (11), $h(t) = t + 1/2$, $s(t) = t^{2/3}$. Noisy observation data were obtained by adding noises from $N(0, \sigma_\epsilon = \sqrt{5}/2)$ to the generated nonstationary GP data (true signals).

We repeated the simulations 100 times, and calculated the RMSEs of the estimates of signals $\{Z_i(\mathbf{t})\}$, mean function $\mu_Z(\mathbf{t})$, covariance surface $\Sigma_Z(\mathbf{t}, \mathbf{t})$, and residual variance σ_ϵ^2 (\mathbf{t} denotes the common observation grid). The average RMSEs (with standard deviations among these 100 simulations) for stationary and nonstationary data were shown in Table 1, where the CSS estimates of (μ_Z, Σ_Z) were sample estimates with pre-smoothed signals by CSS, and average RMSEs were omitted if the parameters were not directly estimated by the corresponding methods, e.g., $(\mu_Z, \Sigma_Z, \sigma_\epsilon^2)$ by BFPCA, σ_ϵ^2 by CSS.

Table 1 shows that BGP produces the best estimates for the signals and residual variance (with the lowest RMSEs), while BHM and BABF gives the second best estimates for the signals and residual variance, as well as the best estimates for the mean-covariance functions. With nonstationary data of common grids, BGP and PACE produce the best covariance estimates, while BABF produces closely accurate covariance estimates, as well as the best estimates for the signals, mean function, and residual variance. Because of stable computations with nonstationary data, our BABF method produces better estimates than BHM. In addition, the CSS and BFPCA methods produce the least accurate estimates (with the highest RMSEs) for both stationary and nonstationary data, which demonstrates the advantage of simultaneously smoothing and estimating functional data as in BGP, BHM, and BABF.

[Table 1 about here.]

Figure 1 (a, b, c, d) shows that all three Bayesian methods produce similarly accurate estimates for the functional signals and mean function of common grids. With nonstationary data, our BABF

method produces the best signal estimates (Figure 1(b)). As for the functional covariance estimates (Supplementary Figure 1), the parametric estimate by BGP is a Matérn function because of the assumed true Matérn covariance model, but with underestimated diagonal variances. Practically, a wrong covariance model is usually assumed in BGP, which is likely to produce estimates with large errors and wrong structures. In contrast, the nonparametric methods such as BHM and BABF are more flexible and applicable for estimating the covariance function of real data.

In addition, we examined the coverage probabilities of the 95% pointwise credible intervals (CI) generated by BGP, BHM, and BABF, for the functional signals and mean-covariance functions (Supplementary Table 1). For functional signals, BGP results the highest coverage probability with stationary data (0.9483 vs. 0.9217, 0.9208), but the lowest coverage probability with nonstationary data (0.8350 vs. 0.9450, 0.8742). All methods have similar coverage probabilities for the functional mean (~ 0.7), where the relatively low coverage probabilities are due to the narrow 95% confidence intervals. As for the covariance, the coverage probability by BGP is significantly lower than the ones by BHM and BABF for both stationary (0.000 vs. 0.7869, 0.7869) and nonstationary data (0.3819 vs. 0.9913, 0.9938), because BGP underestimates the diagonal variances.

In summary, with common grids, Bayesian GP based regression methods (BGP, BHM, and BABF) produce better smoothing and estimation results, compared to estimating mean-covariance functions using the pre-smoothed functional data by CSS. Moreover, the results by BABF are at least similar to the ones by the original BHM, and better with nonstationary data.

3.2 Studies with random grids

For this set of simulations, we generated 30 true functional curves from the stationary and non-stationary GPs as in Section 3.1, with observational grids (length 40) that were randomly (uniformly) generated over $\mathcal{T} = (0, \pi/2)$. Raw functional data were then obtained by adding noises from $N(0, \sqrt{5}/2)$ to the true signals. We compared our BABF method (using an equally spaced working grid $\tau_{1 \times 20} \subset \mathcal{T}$) with CSS and PACE, by 100 simulations.

Table 2 presents the average RMSEs for the estimates of the signals, residual variance, and mean-covariance functions (evaluated on the equally spaced grid over \mathcal{T} with length 40), along with standard errors in the parentheses. It is shown that our BABF method (with lowest RMSEs) performs consistently better than CSS and PACE for signal and mean estimates, with both stationary and nonstationary data of random grids.

[Table 2 about here.]

[Figure 1 about here.]

Figure 1 (e, f) shows that BABF produces the best signal estimates in the scenario with random grids. This is because CSS smoothed each functional curve independently; PACE only uses limited information per pooled-grid point; while BABF borrows strength across all observations through basis function approximations. For both stationary and nonstationary functional data, PACE and BABF give closely accurate mean estimates, while CSS gives the least accurate mean estimate (Figure 1 (g, h)). In addition, PACE produces the roughest covariance estimate (Supplementary Figure 2), for only using limited information on the pooled-grid points. The BABF coverage probability of the covariance is 0.9506 for stationary data and 0.8550 for nonstationary data, showing the good performance of our BABF method.

In summary, with random grids, our BABF method produces the best signal and mean estimates, compared to CSS and PACE. Although the sample covariance estimate using the pre-smoothed data generated by CSS has the lowest RMSE for nonstationary data, the analogous estimate using the more accurately smoothed data generated by BABF will have at least similar RMSE.

3.3 Studies about robustness

To test the robustness of our BABF method for handling non-Gaussian data, we further simulated stationary functional data from a non-Gaussian process, $0.2(X(t)^2 - 1) + X(t)$, which is a modified Hermite polynomial transformation of the GP $X(t)$ in (11). We simulated functional data with

$n = 30$, random grids ($p = 40$) over $\mathcal{T} = (0, \pi/2)$, and noises from $N(0, \sqrt{5}/2)$. Compared to CSS, our BABF method has RMSE 0.4278 vs. 0.7092 for the signal estimates, 0.1271 vs. 0.4992 for the functional mean estimate, and 0.4417 vs. 0.8886 for the functional covariance estimate. These results demonstrate that our BABF method is robust for analyzing non-Gaussian functional data. In addition, we note that it is crucial to select a correct prior structure, $A(\cdot, \cdot)$ in (1), for the functional covariance. In general, we suggest using the Matérn model for stationary data and a smoothed covariance estimate by PACE for nonstationary data.

3.4 Goodness-of-fit diagnostics

We applied the method of goodness-of-fit (Yuan and Johnson, 2012) using pivotal discrepancy measures (PDMs) on the residuals, $\epsilon_i(t) = Y_i(t) - Z_i(t)$, to examine the global goodness-of-fit of the Bayesian hierarchical model (1). As functions of the data and model parameters, the PDMs have the same invariant distribution when evaluated at the data-generating parameter value and parameter values drawn from the posterior distribution. Following the method proposed by Yuan and Johnson (2012), we constructed PDMs using standardized residuals from the posterior samples in MCMC. The PDM follows a chi-squared distribution under the null hypothesis that the residuals follow the $N(0, \sigma_\epsilon^2)$ distribution (i.e., global goodness-of-fit for the Bayesian hierarchical model). In all simulation studies, the p-values of testing the null hypothesis of global goodness-of-fit for the Bayesian hierarchical model are greater than 0.25, providing no evidence of lack-of-fit.

4. Application on real data

We analyzed a functional dataset from an obesity study with children and adolescents (Lee et al., 2016), by the Children's Nutrition Research Center (CNRC) at Baylor College of Medicine. This study estimated the energy expenditure (EE in unit kcal) of 106 children and adolescents (44 obese cases, 62 nonobese controls) during 24 hours with a series of scheduled physical activities and a sleeping period (12:00am-7:00am), by using the CNRC room respiration calorimeters (Moon et al.,

1995). We only analyzed the sleeping energy expenditure (SEE) data measured at 405 time points during the sleeping period. This real SEE data set provides a good example of high-dimensional common grids. The goal of this study was to discover different data patterns between obese cases and controls, providing insights about obesity diagnosis.

We applied CSS, PACE, and our BABF method on this SEE functional data. Specifically, CSS was applied independently per sample with a smoothing parameter selected by GCV; PACE was applied with common grid $[1 : 405]$; and BABF was applied with the equally spaced working grid over $[1 : 405]$ with length 30. Both PACE and BABF were applied separately for the functional data of obese and nonobese groups. Figure 2 (a, b) shows that CSS produces the roughest signal estimates, leading to the roughest mean-covariance estimates (Figures 2 (c, d); Supplementary Figures 3 and 4). Both PACE and BABF produce smoothed signal estimates and mean-covariance estimates. The mean estimate by BABF has better periodic patterns than the one by PACE (Figures 5 (c, d)), and the BABF estimates of the correlations between two apart time points are less than the PACE estimates (Supplementary Figure 4).

[Figure 2 about here.]

Further, we applied the goodness-of-fit test (Yuan and Johnson, 2012) to the residuals from the BABF method (one test per functional sample). Although the residual means are consistently close to 0, the p-values for 52% functional curves are less than $0.05/n$, suggesting evidences of lack-of-fit with Bonferroni correction (Bonferroni, 1936) for multiple testing. This is because the residual variances of this real data are no longer the same across all observations. To address the issue of lack-of-fit for this SEE data, we need to assume sample-specific residual variances in the Bayesian hierarchical model (1), which is beyond the scope of this paper but will be part of our future research.

Despite the lack-of-fit issue for this real data application by BABF, the smoothed data by BABF are improved over the raw data and the smoothed data by alternative methods for follow-up

analyses. Using classification analysis as an example, we next illustrate the advantage of using the smoothed data by BABF for follow-up analyses. Considering the SEE data of obese and nonobese children as two classes, we used the leave-one-out cross-validation (LOOCV) approach to evaluate the classification results for using the raw data, and the smoothed data by CSS, PACE, and BABF. Basically, for each sample curve, we trained a SVM model (Cortes and Vapnik, 1995) using the other sample curves, and then predicted if the test sample was an obese case. The error rate (the proportion of misclassification out of 106 samples) is 48.11% for using the raw data, 40.57% for using the smoothed data by CSS, and 36.79% for using the smoothed data by PACE, and 33.02% for using the smoothed data by BABF. The smoothed data by our BABF method lead to the smallest error rate. Thus, we believe using the smoothed data by BABF will be useful for follow-up analyses.

5. Discussion

In this paper, we propose a computational efficient Bayesian method (BABF) for smoothing and estimating mean-covariance functions of high-dimensional functional data, improving upon the previous BHM method by Yang et al. (2016). Our BABF method projects the original functional data onto the space of selected basis functions with reduced rank, and then conducts posterior inference through MCMC of the basis-function coefficients. As a result, BABF method not only retains the same advantages as BHM, such as simultaneously smoothing and estimating mean-covariance functions in a nonparametric way, but also provides additional computational advantages of scalability, efficiency, and stability. A software for implementing the BHM and BABF methods is freely available at <https://github.com/yjingj/BFDA> (Yang and Ren, 2016).

With n functional observations, a pooled observation grid of dimension p , and m MCMC iterations, BABF reduces the computational complexity from $O(np^3m)$ to $O(nK^3m)$, and the memory usage from $O(p^2m)$ to $O(K^2m)$, by MCMC in the basis-function space with reduced

rank $K \ll p$. For examples, using a 3.2 GHz Intel Core i5 processor, BABF only costs about 3 minutes for $n = 30$, $K = 20$, and $m = 12,000$, and about 9 minutes for $n = 44$, $K = 30$, and $m = 12,000$. Although BABF (with 12,000 MCMC iterations) costs about 4x longer than PACE, BABF provides complementary credible intervals to quantify the uncertainties of the posterior estimates, as well as basis function representations for the nonparametric estimates of functional signals and mean-covariance functions. Moreover, BABF produces more accurate results than PACE for functional data observed on random grids.

Both simulation and real studies demonstrate that BABF performs similarly as BHM and other Bayesian GP regression methods with functional data observed on low-dimensional common grids, and that BABF outperforms the alternative methods (e.g., CSS, PACE) with functional data observed on random grids or high-dimensional common grids. In addition, the real application shows that the classification analysis using the smoothed data by BABF produces the most accurate results.

BABF assumes the same mean-covariance functions and residual variance for functional data, both of which are not true for most of the real data. Despite the model inadequacy, the smoothed data by BABF are still useful for follow-up analyses as shown in the real application of SEE data. To make the method more flexible for real data analysis, one might assume group-specific mean-covariance functions and sample-specific residual variances. This is beyond the scope of this paper and will be part of our future research.

In conclusion, BABF greatly improves the computational scalability and decreases the memory usage upon the original BHM method, while efficiently smoothing functional data and estimating mean-covariance functions in a nonparametric way. By implementing MCMC with the induced model of basis-function coefficients, our novel basis function approximation approach provides one solution for the computational bottleneck of general Bayesian GP regression methods, especially for analyzing high-dimensional functional data with Gaussian-Wishart processes.

Acknowledgments

The authors would like to thank the Children’s Nutrition Research Center at the Baylor College of Medicine for providing the metabolic SEE data (funded by National Institute of Diabetes and Digestive and Kidney Diseases Grant DK-74387 and the USDA/ARS under Cooperative Agreement 6250-51000-037). The authors would like to thank the writing lab of the School of Public Health at University of Michigan for helping proofread this manuscript. Jingjing Yang and Dennis D. Cox were supported by the NIH grant PO1-CA-082710.

References

- Baladandayuthapani, V., Mallick, B. K., Young Hong, M., Lupton, J. R., Turner, N. D., and Carroll, R. J. (2008). Bayesian hierarchical spatially correlated functional data analysis with application to colon carcinogenesis. *Biometrics* **64**, 64–73.
- Banerjee, A., Dunson, D. B., and Tokdar, S. T. (2013). Efficient Gaussian process regression for large datasets. *Biometrika* **100**, 75–89.
- Banerjee, S., Gelfand, A. E., Finley, A. O., and Sang, H. (2008). Gaussian predictive process models for large spatial data sets. *Journal of the Royal Statistical Society: Series B (Statistical Methodology)* **70**, 825–848.
- Bonferroni, C. E. (1936). Teoria statistica delle classi e calcolo delle probabilita. *Pubblicazioni del R Istituto Superiore di Scienze Economiche e Commerciali di Firenze* **8**, 3–62.
- Cardot, H., Ferraty, F., and Sarda, P. (1999). Functional linear model. *Statistics & Probability Letters* **45**, 11–22.
- Cardot, H., Ferraty, F., and Sarda, P. (2003). Spline estimators for the functional linear model. *Statistica Sinica* **13**, 571–592.
- Cortes, C. and Vapnik, V. (1995). Support-vector networks. *Machine learning* **20**, 273–297.
- Crainiceanu, C. M. and Goldsmith, A. J. (2010). Bayesian functional data analysis using winbugs.

- Journal of Statistical Software* **32**, 11.
- Cressie, N. and Johannesson, G. (2008). Fixed rank kriging for very large spatial data sets. *Journal of the Royal Statistical Society: Series B (Statistical Methodology)* **70**, 209–226.
- Dawid, A. P. (1981). Some matrix-variate distribution theory: notational considerations and a bayesian application. *Biometrika* **68**, 265–274.
- de Boor, C. (1977). Computational aspects of optimal recovery. In Micchelli, C. A. and Rivlin, T. J., editors, *Optimal Estimation in Approximation Theory*, pages 69–91. Springer US, Boston, MA.
- Fan, Y., James, G. M., and Radchenko, P. (2015). Functional additive regression. *Ann. Statist.* **43**, 2296–2325.
- Ferraty, F. and Vieu, P. (2006). *Nonparametric functional data analysis: theory and practice*. Springer-Verlag New York.
- Finley, A., Banerjee, S., and Gelfand, A. (2015). spBayes for large univariate and multivariate point-referenced spatio-temporal data models. *Journal of Statistical Software* **63**, 1–28.
- Gaffney, P. W. and Powell, M. J. D. (1976). *Optimal interpolation*. Springer Berlin Heidelberg.
- Gelman, A. and Rubin, D. B. (1992). Inference from iterative simulation using multiple sequences. *Statistical Science* **7**, 457–472.
- Geman, S. and Geman, D. (1984). Stochastic relaxation, gibbs distributions, and the bayesian restoration of images. *Pattern Analysis and Machine Intelligence, IEEE Transactions on* **6**, 721–741.
- Gibbs, M. N. (1998). *Bayesian Gaussian processes for regression and classification*. PhD thesis, University of Cambridge, UK.
- Green, P. J. and Silverman, B. W. (1993). *Nonparametric regression and generalized linear models: a roughness penalty approach*. CRC Press.
- Gromenko, O. and Kokoszka, P. (2013). Nonparametric inference in small data sets of spatially

- indexed curves with application to ionospheric trend determination. *Computational Statistics & Data Analysis* **59**, 82–94.
- Hall, P., Horowitz, J. L., et al. (2007). Methodology and convergence rates for functional linear regression. *The Annals of Statistics* **35**, 70–91.
- James, M. (1978). The generalised inverse. *The Mathematical Gazette* **62**, 109–114.
- Kaufman, C. G. and Sain, S. R. (2010). Bayesian functional ANOVA modeling using gaussian process prior distributions. *Bayesian Analysis* **5**, 123–149.
- Lee, J. S., Zakeri, I. F., and Butte, N. F. (2016). Functional principal component analysis and classification methods applied to dynamic energy expenditure measurements in children. *Technical Report*.
- Matérn, B. (1960). *Spatial variation. Stochastic models and their application to some problems in forest surveys and other sampling investigations*. PhD thesis, Meddelanden fran Statens Skogsforskningsinstitut.
- Micchelli, C. A., Rivlin, T. J., and Winograd, S. (1976). The optimal recovery of smooth functions. *Numerische Mathematik* **26**, 191–200.
- Moon, J. K., Vohra, F. A., Valerio Jimenez, O. S., Puyau, M. R., and Butte, N. F. (1995). Closed-loop control of carbon dioxide concentration and pressure improves response of room respiration calorimeters. *Journal of Nutrition-Baltimore and Springfield then Bethesda* **125**, 220–220.
- Quiñonero Candela, J., E., R. C., and Williams, C. K. I. (2007). Approximation methods for gaussian process regression. Technical report, Applied Games, Microsoft Research Ltd.
- Ramsay, J. O. and Dalzell, C. (1991). Some tools for functional data analysis. *Journal of the Royal Statistical Society. Series B (Methodological)* **53**, 539–572.
- Ramsay, J. O. and Silverman, B. W. (2005). *Functional data analysis*. Springer Series in Statistics. Springer, New York, second edition.

- Rasmussen, C. E. and Williams, C. K. I. (2006). *Gaussian Processes for Machine Learning*. Adaptive Computation and Machine Learning. MIT Press, Cambridge, MA.
- Sang, H. and Huang, J. Z. (2012). A full scale approximation of covariance functions for large spatial data sets. *Journal of the Royal Statistical Society: Series B (Statistical Methodology)* **74**, 111–132.
- Scheipl, F., Staicu, A.-M., and Greven, S. (2015). Functional additive mixed models. *Journal of Computational and Graphical Statistics* **24**, 477–501.
- Shi, J., Wang, B., Murray-Smith, R., and Titterton, D. (2007). Gaussian process functional regression modeling for batch data. *Biometrics* **63**, 714–723.
- Shi, J. Q. and Choi, T. (2011). *Gaussian process regression analysis for functional data*. Chapman and Hall/CRC.
- Yang, J. and Ren, P. (2016). BFDA: A matlab toolbox for bayesian functional data analysis. *arXiv preprint arXiv:1604.05224* .
- Yang, J., Zhu, H., Choi, T., and Cox, D. D. (2016). Smoothing and meancovariance estimation of functional data with a bayesian hierarchical model. *Bayesian Analysis* **11**, 649–670.
- Yao, F., Müller, H.-G., and Wang, J.-L. (2005a). Functional data analysis for sparse longitudinal data. *Journal of the American Statistical Association* **100**, 577–590.
- Yao, F., Müller, H.-G., and Wang, J.-L. (2005b). Functional linear regression analysis for longitudinal data. *The Annals of Statistics* **33**, 2873–2903.
- Yuan, Y. and Johnson, V. E. (2012). Goodness-of-fit diagnostics for bayesian hierarchical models. *Biometrics* **68**, 156–164.
- Zhu, H., Brown, P. J., and Morris, J. S. (2011). Robust, adaptive functional regression in functional mixed model framework. *Journal of the American Statistical Association* **106**, 1167–1179.
- Zhu, H. and Cox, D. D. (2009). A functional generalized linear model with curve selection in cervical pre-cancer diagnosis using fluorescence spectroscopy. In *Optimality: The Third Erich*

L. Lehmann Symposium, volume 57 of *Lecture Notes Monograph Series*, pages 173–189.

Institute of Mathematical Statistics, Beachwood, OH, USA.

Zhu, H., Yao, F., and Zhang, H. H. (2014). Structured functional additive regression in reproducing kernel hilbert spaces. *Journal of the Royal Statistical Society: Series B (Statistical Methodology)* **76**, 581–603.

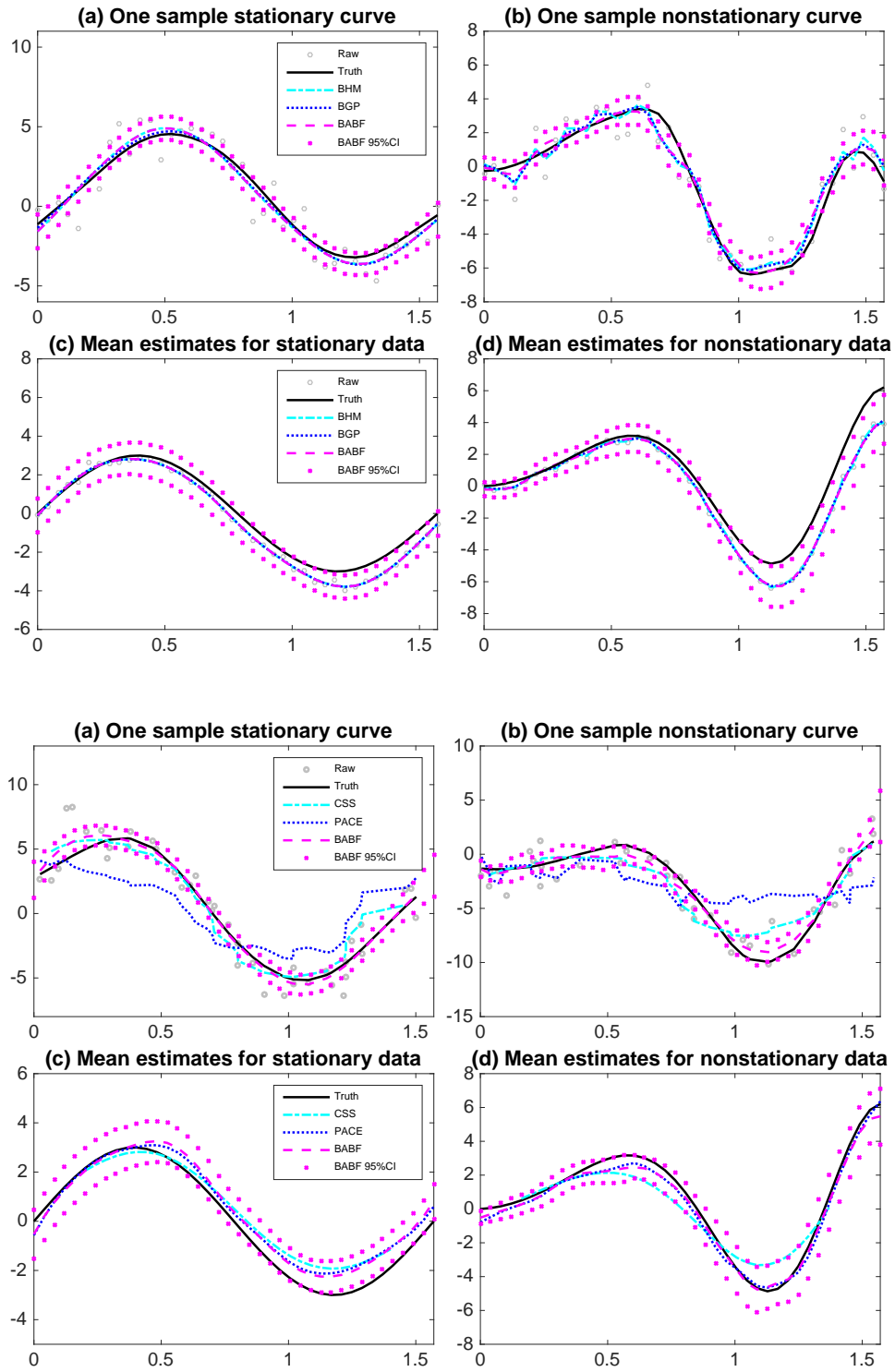


Figure 1. Example smoothed functional data of common grids in (a, b), mean estimates of common grids in (c, d), example smoothed functional data of random grids in (e, f), and mean estimates of random grids in (g, h), along with 95% pointwise CIs by BABF.

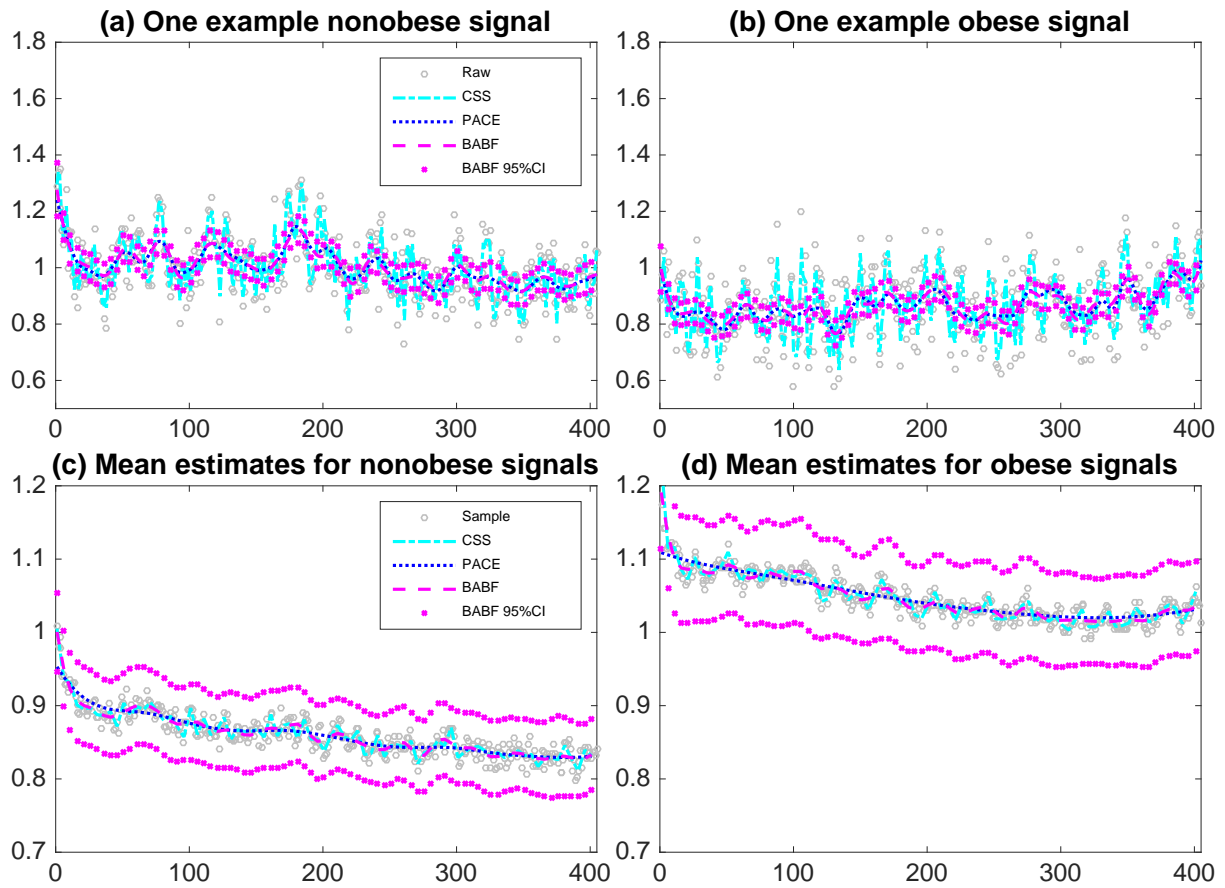


Figure 2. Example smoothed functional data in (a, b) and mean estimates in (c, d), along with 95% pointwise CIs by BABF, for the real SEE data.

Table 1

Simulation results with common grids: average RMSEs and corresponding standard errors (in parentheses) of $\{Z_i(\mathbf{t})\}$, $\mu(\mathbf{t})$, $\Sigma_Z(\mathbf{t}, \mathbf{t})$, and σ_ϵ^2 produced by CSS, PACE, BFPCA, BGP, BHM, and BABF. Average RMSEs are omitted if the corresponding parameters are not directly estimated. Two best results are bold for each parameter.

	CSS	PACE	BFPCA	BGP	BHM	BABF
Stationary						
$\{Z_i(\mathbf{t})\}$	0.4808 (0.0213)	0.4553 (0.0268)	0.5657 (0.0550)	0.4020 (0.0219)	0.4067 (0.0207)	0.4073 (0.0204)
$\mu(\mathbf{t})$	0.4757 (0.1347)	0.4194 (0.1593)	-	0.3982 (0.1527)	0.3961 (0.1538)	0.3961 (0.1535)
$\Sigma(\mathbf{t}, \mathbf{t})$	1.0017 (0.3079)	1.0375 (0.2850)	-	1.0988 (0.4934)	0.9601 (0.2902)	0.9590 (0.2913)
σ_ϵ^2	-	0.0764 (0.0516)	-	0.0460 (0.0327)	0.0491 (0.0357)	0.0483 (0.0352)
Nonstationary						
$\{Z_i(\mathbf{t})\}$	1.0271 (0.00463)	0.5185 (0.0255)	0.6314 (0.0632)	0.5183 (0.0265)	0.5759 (0.0227)	0.5133 (0.0227)
$\mu(\mathbf{t})$	0.9446 (0.1509)	0.5782 (0.2095)	-	0.5387 (0.2090)	0.5530 (0.2038)	0.5356 (0.2094)
$\Sigma(\mathbf{t}, \mathbf{t})$	1.9635 (0.8386)	1.9751 (0.8160)	-	1.9733 (0.6831)	2.0296 (0.6891)	1.9768 (0.7835)
σ_ϵ^2	-	0.0810 (0.0541)	-	0.1472 (0.0879)	0.2432 (0.0644)	0.0692 (0.0492)

Table 2

Simulation results with random grids: average RMSEs and corresponding standard errors (in parentheses) of $\{Z_i(\mathbf{t})\}$, $\mu(\mathbf{t})$, $\Sigma_Z(\mathbf{t}, \mathbf{t})$, and σ_ϵ^2 by CSS, PACE, and BABF. Average RMSEs are omitted if the corresponding parameters are not directly estimated. Best results are bold for each parameter.

	Stationary			Nonstationary		
	CSS	PACE	BABF	CSS	PACE	BABF
$\{Z_i(\mathbf{t})\}$	0.4839 (0.0229)	1.4141 (0.1424)	0.4079 (0.0219)	1.0137 (0.0511)	2.6300 (0.2876)	0.6832 (0.0576)
$\mu(\mathbf{t})$	0.4229 (0.1471)	0.4196 (0.1290)	0.3690 (0.1302)	0.9905 (0.1888)	0.6157 (0.2160)	0.5920 (0.2138)
$\Sigma(\mathbf{t}, \mathbf{t})$	1.0445 0.4313	1.4089 (0.3502)	1.0054 (0.3286)	1.6403 (0.6086)	2.4120 (0.6497)	2.2090 (0.4506)
σ_ϵ^2	- -	0.1900 (0.1818)	0.0509 (0.0387)	- -	0.4007 (0.2960)	0.2209 (0.1189)